AU8910383

UM-P-89/11

CHARACTERIZATION OF NANOCRYSTALLINE ZIRCONIA POWDERS BY ELECTRON OPTICAL TECHNIQUES

L.A. BURSILL [1,2] E. BERNSTEIN [2] and M.G. BLANCHIN [2]

1. School of Physics, University of Melbourne, 3052, VIC, AUSTRALIA

2. Département de Physique des Matériaux, Université Claude Bernard Lyon I, 43 Bd du 11 novembre 1918, 69622 VILLEURBANNE, CEDEX, FRANCE

ABSTRACT

Electron optical techniques are described for the characterization of the size distribution of agglomerates, aggregates and primary micro-and nanocrystallites of as-processed zirconia powders. These techniques allow for direct identification of individual crystallites as tetragonal or monoclinic, by optical transform of high-resolution electron micrographs. The latter also permit surface morphology to be examined with atomic resolution.

Application to a range of pure and doped zirconia powders, of recent commercial interest, are presented, which enable the results of concurrent studies by sedimentation, surface specific area measurements, porosity and sinterability to be correctly interpreted.

1 INTRODUCTION

The use of microcrystalline (submicron) and nanocrystalline (10 nm) particles as precursor materials for fabrication of advanced ceramics, for examole high temperature superconductors as well as oxide-based ceramics, requires new techniques for characterization. Thus classical optical mircroscopy (resolution $\simeq$ 1 μm) or even scanning electron microscopy (resolution $\simeq$ 5-10 nm) are no longer effective for examination of 1-10 nm particles. At the Département de Physique des Matériaux, Université Claude Bernard, we have developed techniques appropriate for the direct determination of the morphology, size, homogeneity and states of aggregation, agglomeration or floculation of ceramic powders. The onset of sintering may be sensitively detected and porosity may be visualized down to the nanometre scale. In addition the atomic structure of vicinal surfaces and facets, as well as intergranular interfaces may be explored with respect to variation of processing route (chemical and physical parameters). Observations of zirconia powders of recent industrial interest are summarized below. These emphasize the potential contribution of transmission electron microscopy (T.E.M.) at medium resolution, as well as transmission high-resolution electron microscopy (H.R.E.M), for the routine analysis of

.../...

ultrafine ceramic powders. These techniques act as both complementary to existing characterization techniques, as well as providing quite new types of information.

2. SIZE DISTRIBUTION OF PARTICLES

Two zirconia powders were prepared [1] by calcination of crystallized acetates (C) and amorphous acetates (A). Preliminary characterization included determination of the size distribution of weakly-bonded agglomerates by sedimentation, measurement of the specific surface areas by B.E.T and of the mean crystallite sizes by X-ray diffractometry. The powders were then examined by TEM [2]. For example, Fig. 1a,b compares these two powders at low magnification, following dispersion of dry powder onto a transparent carbon support film. Individual particles range in size from $0.05\ \mu m \leqslant D \leqslant 0.7 \mu m$ for specimen A and $0.05\ \mu m \leqslant D \leqslant 1.5\ \mu m$ for specimen C.

Sedimentation measurements using a centrifugal particle size distribution analyzer and "optimal dispersion conditions" yielded agglomerate dimensions $0.5\ \mu m \leqslant D(A) \leqslant 8\ \mu m$ for A and $0.5\ \mu m \leqslant D(C) \leqslant 3\ \mu m$ for C. The surface area results were 6.2 m^2/g for A and 12.2 m^2/g for C, corresponding to equivalent spherical diameters Ds = 160 nm for A and 80 nm for C respectively [1]. Conventional TEM, using both bright and

.../...

dark-field imaging modes, as well as electron diffraction [3] showed clearly that powder A forms weakly-bondeo agglomerates of primary crystalline particles (see fig. 1c). whereas powder C formed both strongly-bonded aggregates of primary crystallites as well as agglomerates of the latter (see fig. 1 d). A HREM image [4] of powder C (fig. 2) clearly reveals the polycrystalline nature of such an aggregate. The lattice fringes [4] having different spacings (0.2-0.5 nm) and orientations, reveal the extent of the primary crystallites as well as the crystallite boundaries. Obviously the unusual aggregates of this powder tend to have a platelet habit, with some preferred alignment of primary crystallites. These should be compared to the loosely-bonded agglomerates of powder A, composed of distinct polyhedra (see fig. 1 c and d). The difference may be attributed to the different chemical processing routes, via crystalline and amorphous acetates respectively, since the calcination temperatures were identical.

Note that the distribution of secondary particles (aggregates or agglomerates), as determined by TEM was much narrower than that measured by sedimentation techniques ; which proves that even if the dispersive conditions are optimized (by controlling the pH of the dispersing liquid), zirconia remains heavily agglomerated in solution. Consequently, as described above, the particle size analyzer does not necessarily give either the size of the agglomerates or aggregates existing in the original dry powder preparations. Equivalent spherical diameters, calculated from specific surface area measurements have also to be examined with caution. In the case of powder A, the primary particles may be considered as approximately spherical, but they present a wide size distribution, with diameters determined by TEM ranging from 22 nm-250 nm. Powder C is

.../...

formed rather of plate-shaped aggregates, approx. 30 nm thick, as determined by tilting experiments in the TEM. For the latter case the equivalent spherical diameter, obtained from B.E.T. measurements, has little physical relevance. Furthermore the high resolution image of powder C (fig. 2) shows that the surface area is greatly increased by extensive pitting of the surface, as well as by the appearance of vicinal surface steps in the surface profile. Thus the effects of aggregation of primary crystallites is partially counteracted by surface roughening of individual crystallites ; again implying caution with respect to interpretation of the B.E.T. measurements.

3. EFFECT OF CALCINATION TEMPERATURE

Ultrafine zirconia powders were processed by calcination of an amorphous hydrated zirconia oxide at temperatures between 300°C and 1100°C (see table I for values of typical ceramic parameters X-ray examination showed the sequence

amorphous $\xrightarrow{350°C}$ tetragonal $\xrightarrow{550°C}$ monoclinic

with increasing temperature. Figs 3a-c reproduce three HREM images obtained for samples calcined for 1 hour at 400°C, 700°C and 800°C respectively. Thus the crystal lattices of whole primary grains have been imaged at 0.22 nm resolution. As well the surface profiles have been obtained, providing a new scale of morphological information. The set of images reveals correlated changes in crystallite sizes and development of surface facetting. With increasing temperature the crystallites change from roughly spherical to strongly polyhedral in shape, with a preference for relatively extensive facetting along $(111)_M$ and $(010)_M$ planes (fig. 3b). As well the crystal structure changes from predominantly tetragonal to predominantly monoclinic.

.../...

4. IDENTIFICATION OF CRYSTALLINE MODIFICATION

Optical diffractograms, obtained by forming the Fraunhofer diffraction pattern of the images using laser illumination on an optical bench [4], allow the symmetry and reciprocal lattice geometry of the crystallites to be determined, even for single nanocrystalline grains of diameter $\leqslant 10$ nm like in fig. 3a. This proved to be a powerful tool for identifying the tetragonal and/or monoclinic phases of zirconia. Thus diffractograms of fig. 4a, b show $[100]_T$ and $[111]_T$ orientations of tetragonal zirconia for the areas labelled A and B in fig. 3a, whereas figs.4c , d identify $[\bar{1}01]_M$ and $[\bar{1}10]_M$ orientations of the monoclinic phase for areas C and D of figs. 3b, c respectively.

5. ATOMIC SURFACE STRUCTURAL INFORMATION

It is clear from fig. 3a, b, c that much detailed information concerning the atomic surface topology is available from the HREM images. Thus, whereas the tetragonal phase (from a specimen calcined at 400°) contained roughly circular nanocrystals, with a uniformly high distribution of vicinal steps, the monoclinic phase at 700 and 800°C exhibited marked development of $(111)_M$ and $(010)_M$ facets, imposing a more polyhedral habit for the crystalline grains.

Even within the monoclinic phase details of the surface morphology vary significantly, depending on the preparation route. For example, two powders were examined [5], exhibiting specific surface areas of 6.5 m^2/g and 20.6 m^2/g respectively after calcination at identical temperatures. The first showed relatively large, facetted microcrystals, whereas the second had extensive surface roughening associated with the vicinal surfaces of essentially spherical crystallites.

.../...

Such differences are expected to be important for understanding surface reactivity and sintering rates, as well as understanding and interpreting the classical B.E.T. results.

6. TWIN BOUNDARIES

Structural defects are readily apparent in HREM images. Thus fig. 5 shows a twin boundary in a monoclinic grain of a powder processed as described in section 3 but from a different precursor calcined at 1000°C for 1 hour. Such twin boundaries occurred relatively frequently at that temperature but were absent from powders processed from acetate calcined at 950°C for 12 hours.

Crystallographic studies of the microscopic twinning elements, whereby screw axes and/or glide twins may be distinguished from rotation or mirror twins are proceeding using a series of HREM images obtained for different axial projections.

The atomic structure of the twins is interesting from the point of view of understanding the mechanism of tetragonal $\longrightarrow$ monoclinic structural transformation.

7. INTERGRANULAR INTERFACES AND POROSITY DUE TO SINTERING

Fig. 6 shows a TEM image of a zirconia powder processed from crystallized acetate after calcination at 950° for 12 hours. Note the bubble like nature of the aggregate, with develoment of planar minimal surfaces between many of the grains, and curved bubble shapes at the external surfaces. The grains increase in diameter at the higher temperature and longer calcination times. Note also the appearance of void-space, which basically gives rise to porosity and the less than theoretical densities measured typically for ceramics. It is clear that it will be difficult to fill these spaces, without extensive longer range ionic mobility ($\sim$0.5 μm)..This can only be imposed by the application of elevated temperatures and pressures and/or repeated grinding and sintering.

.../...

Clearly, the observational technique depicted here (at magnifications in the range 20-100,000 X) has the potential to provide a routine analysis in view of understanding details of the mechanism and progress of sintering in individual cases.

8. YTTRIA - STABILIZED TETRAGONAL ZIRCONIA

Fig. 7a shows a TEM image exhibiting the texture of a tetragonal zirconia obtained by thermal decomposition at 950°C of mixed zirconium and yttrium acetates [5]. Comparison with fig.6 shows a similar development of grain size and polyhedral facetting, together with a degree of sintering. However the proportion of void-space is relatively low. Thus this preparation appears to yield a good precursor from the point of view of homogeneity of grain size and yttria content; factors which lead to sinterability of commercial interest [6].

Fig. 7b gives a HREM image of this preparation. It shows a bicrystal formed by sintering of two grains. Note the formation of a reentrant angle. The atomic surface profile exhibits once more the combination of facetting of $\{101\}_T$ planes and increasing frequency of vicinal surface steps required to construct the rounded portions of the grains. Regarding the grain boundary structure it is again apparent that it is timely to begin systematic analyses of the frequency of occurence of relatively low surface energy coincidence site lattices as well as more complex multinodal intergranular structures.

9. EFFECTS OF DIFFERENT PROCESSING ROUTES

After structural and textural studies have been made for a number of preparation conditions, and the image contrast mechanisms understood, then it is reasonable to proceed to use TEM and HREM as tools for the evaluation and optimization of diffe-

.../...

rent preparative routes for chemical and physical processing of ceramic precursor and ceramic products. Thus the structural characteristics of both pure and doped zirconia powders, prepared using hydroxychlor, sulphate, acetate and molten nitrate routes, as well as the effects of washing with isopropanol before sintering, have been investigated in this laboratory [3,5-8]. The effects of dewatering by calcination of amorphous hydrous zirconia on tetragonal phase content of zirconia powders have also been examined using TEM techniques in another laboratory [9].

10. CONCLUSION

The techniques of TEM and HREM are capable of routine application in research and industrial laboratories. Thus specimen preparation methods are relatively trivial for powders.
One hour of HREM time provides images of many thousands of particles, allowing a reasonable statistical analysis to be achieved. On-line image processing techniques have been developed for particle-size and statistical analysis of the distributions, a technique widely used by biologists.
Image digitization using the TV camera usually attached to a HREM, together with Fast-Fourier algorithms and an array processor allows rapid (on-line) collection of the equivalent of the optical transform of HREM images of individual grains. Thus readily interpretable nanodiffraction data, by comparison with standards stored in the computer, may be obtained along with the morphological and surface structure data.
It is worth noting that use of a high-resolution video cassette recorder (VCR) or a video disc greatly reduces the need to use expensive, time-consuming photographic processing and

.../...

storage techniques. Thus the images and Fourier transforms may be conveniently stored and reviewed.

Clearly, the above techniques are capable of further development in the field of ceramic processing. Careful attention to specimen preparation is likely to reveal new combinations of particle size distribution and surface morphologies, of interest for ceramic, as well as catalytic, applications.

REFERENCES

[1] SAMDI, A. Thèse Lyon I, Ordre N° 92/87 ;
SAMDI, A. GROLLIER-BARON, Th ; DURAND, B., and ROUBIN, M., Ann Chim. Fr. I3 (I988) I7I and I88.

[2] HIRSCH, P.B., HOWIE, A., NICHOLSON, R.B., PASHLEY, D.W., and WHELAN, M.J., "Electron Microscopy of Thin Crystals", Butterworths, London (I965).

[3] BERNSTEIN, E., BLANCHIN, M.G., and SAMDI, A., Ceramics Intern. in press (I989).

[4] SPENCE, J.C.H., "Experimental High-Resolution Electron Microscopy",. Clarendon Press, Oxford (I98I) ; pp I2I,278.

[5] BLANCHIN, M.G., BURSILL, L.A. and BERNSTEIN, E., L'Industrie Céramique in press (I989).

[6] SAMDI, A., BERNSTEIN, E., GROLLIER-BARON, Th., DURAND, B., ROUBIN, M and BLANCHIN, M.G., Memoire Scientif. de la Revue de Metallurgie, in press (I988).

[7] BERNSTEIN, E., Thèse LYON I, in preparation (I989).

[8] RAVELLE-CHAPUIS, R. and BLANCHIN, M.G., in preparation (I989)

[9] KOSMAC, T., GOPALKRISHNAN, R., KRASEVEC, V. and KOMAC, M., J. de Physique, Colloq. CI, Suppl. no 2, 47 (I986) CI-43.

FIGURE CAPTIONS

Fig. 1 TEM images showing typical distribution of particles
(a) ZrO_2 powder (A) prepared from amorphous acetate calcined at 850°C.
(b) ZrO_2 powder (C) prepared from crystallized acetate calcined at 950°C.
(c) shows details of a weakly-bounded agglomerate of primary crystallites for powder A ;
(d) gives detail of a strongly-bonded aggregate for powder C.

Fig. 2 HREM image of powder C (cf Fig. 1d). Lattice fringes show extent of individual primary crystallites in the aggregate, as well as details of the surface profile. Note presence of vicinal surfaces and steps having height equal to one interatomic spacing.

Fig. 3 HREM images of zirconia powders calcined at 400°C (a), 700°C (b) and 800°C (c) showing increase in crystallite size with increasing temperature. Note also development of $(111)_M$ and (010) facets in (b) and (c).

Fig. 4 (a) and (b) show optical transforms obtained from areas A and B of fig. 3a, allowing the $[100]_T$ and $[111]_T$ projections of the tetragonal phase to be identified ; (c) and (d) show $[\bar{1}01]_M$ and $[\bar{1}10]_M$ projections of the monoclinic phase to be identified for areas C and D of figs. 3b and c respectively.

Fig. 5 HREM image of a zirconia powder calcined at 1000°C for 1 hour, showing detail of a $(100)_M$ twin boundary.

Fig. 6 TEM image of a zirconia powder calcined at 950°C for 12 hours, showing bubble-like nature of a strongly-bonded aggregate of crystallites (monoclinic phase).

.../...

Note initial stages of sintering, indicated by planer interfaces between grains. Voids are indicated which will contribute to porosity.

Fig.7 (a) TEM image of yttria-doped zircon (stabilized tetragonal) after finally calcining at 950°C. Note homogeneous crystallite size distribution and relative absence of pores (cf. Fig. 6). (b) shows HREM image of a bicrystal formed by sintering of two crystallites symmetrically oriented. Note detail of vicinal surfaces with development of $\{101\}_T$ facets. A reentrant angle is formed naturally (top of figure).

TABLE I

Temperature of calcination (°C)	Specific surface area BET (m2/g)	Phases detected by X-ray diffraction
300	141	Traces of tetragonal (T)
400	112	100 % T
500	63	100 % T
600	25	T+ traces of monoclinic (M)
700	14	60 % T, 40 % M
800	7.7	25 % T, 75 % M
900	6.3	M + traces of T
1000	5.4	100 % M
1100	4.5	100 % M

The proportion of phases represents the ratio T/M and not the total percentage, since there is also an amorphous phase present at low temperatures.

Differential thermal analysis places crystallization temperature at about 430 °C.

Fig 1a

Fig 1b

Fig 1c

Fig 1d

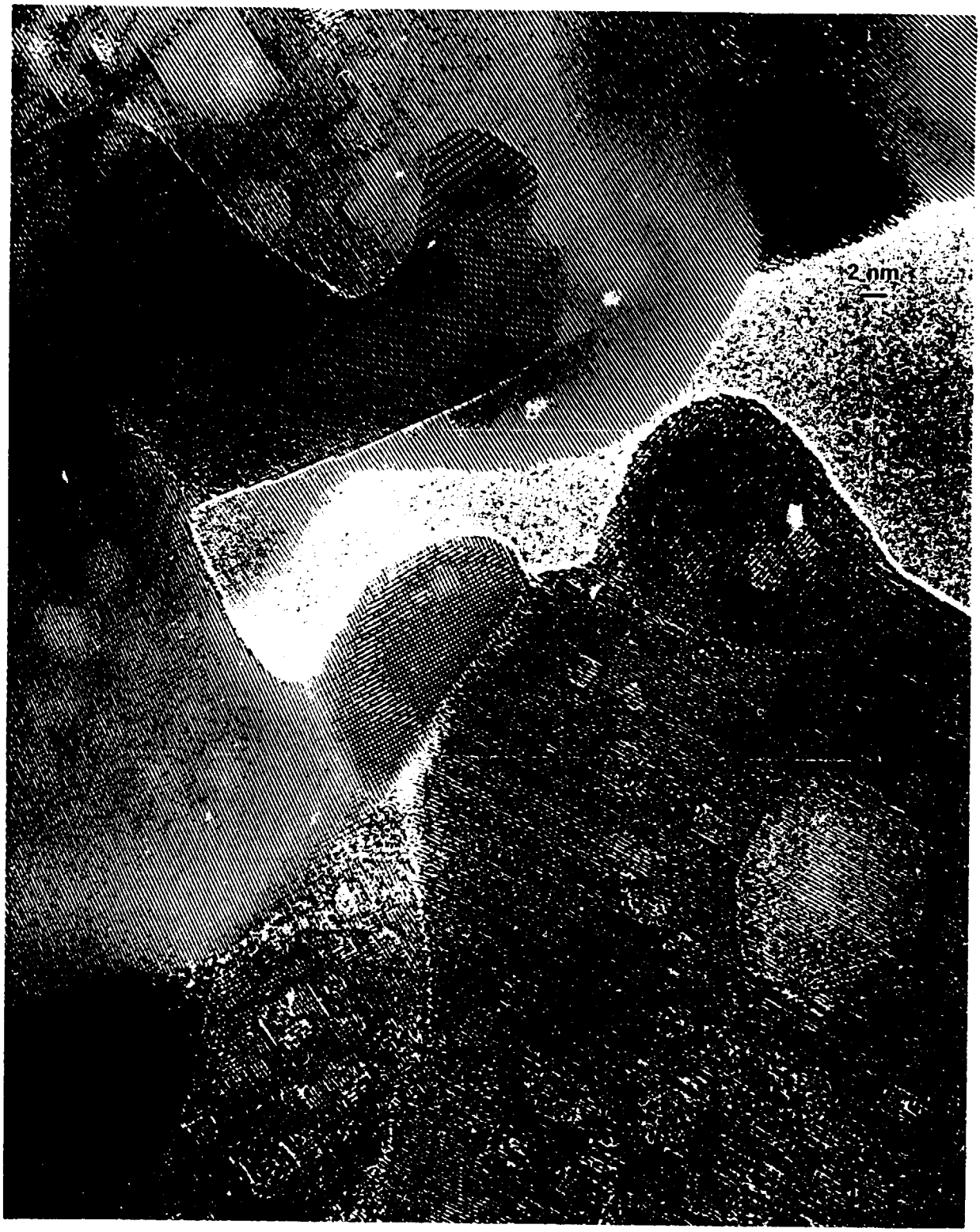

Fig 2.

Fig 3a

Fig 3b

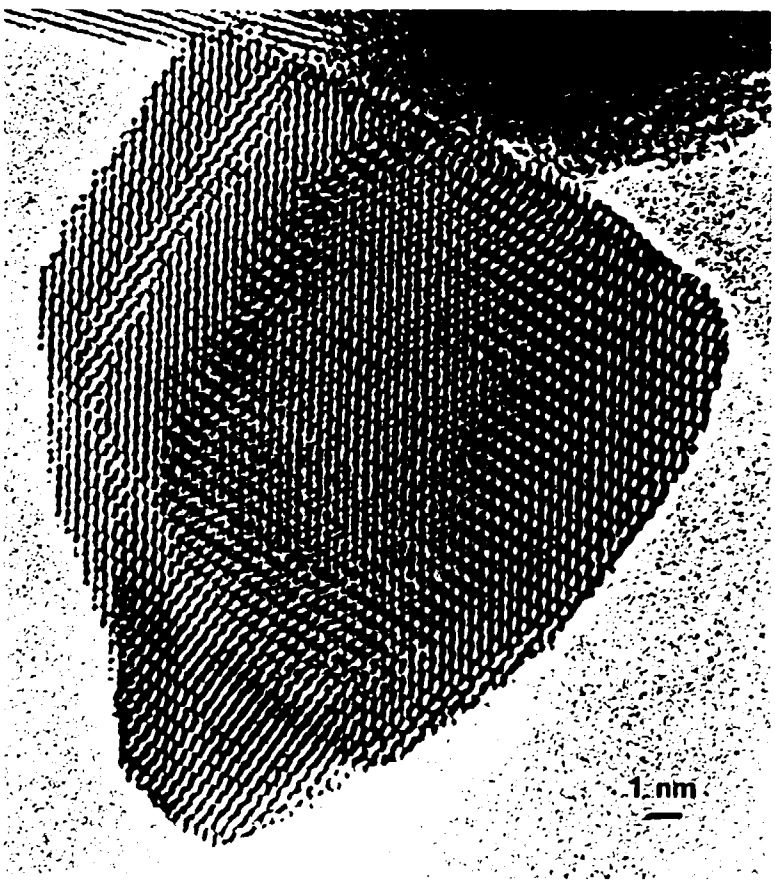

Fig 3c

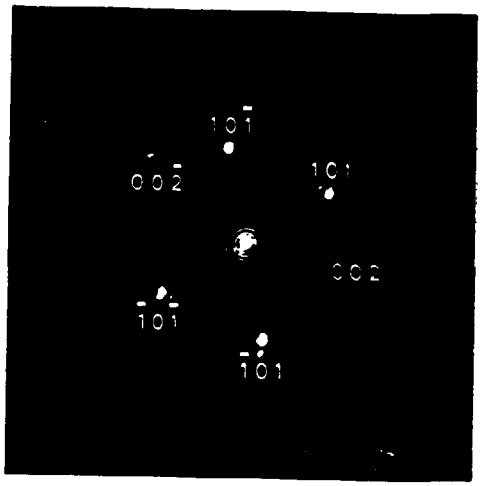

Fig 4a

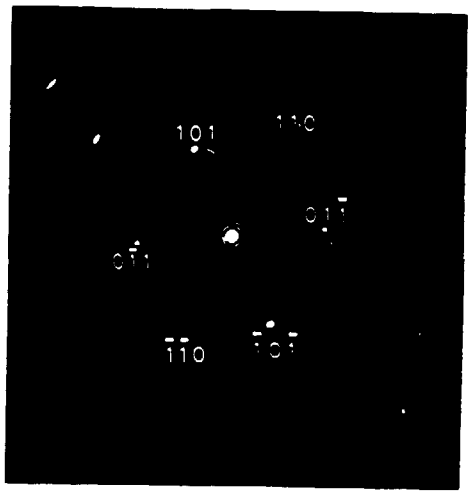

Fig 4b

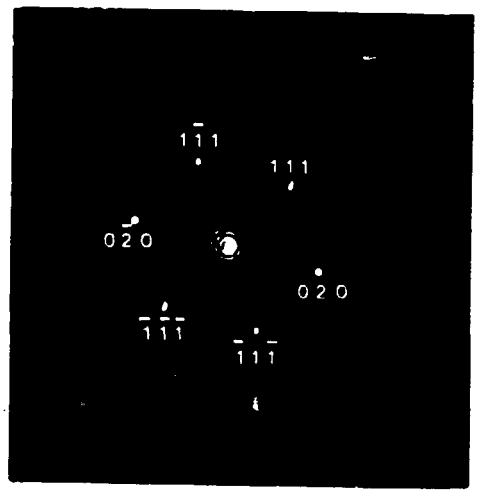

Fig 4c

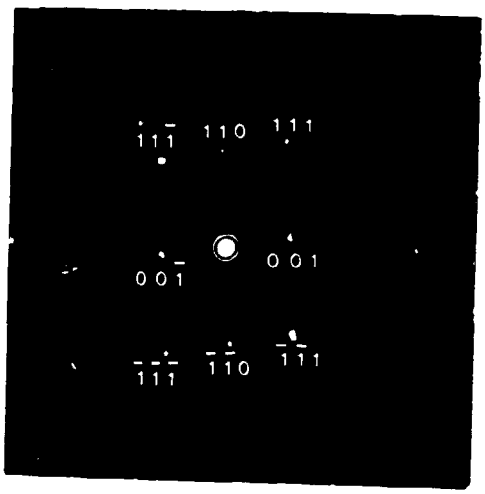

Fig 4d

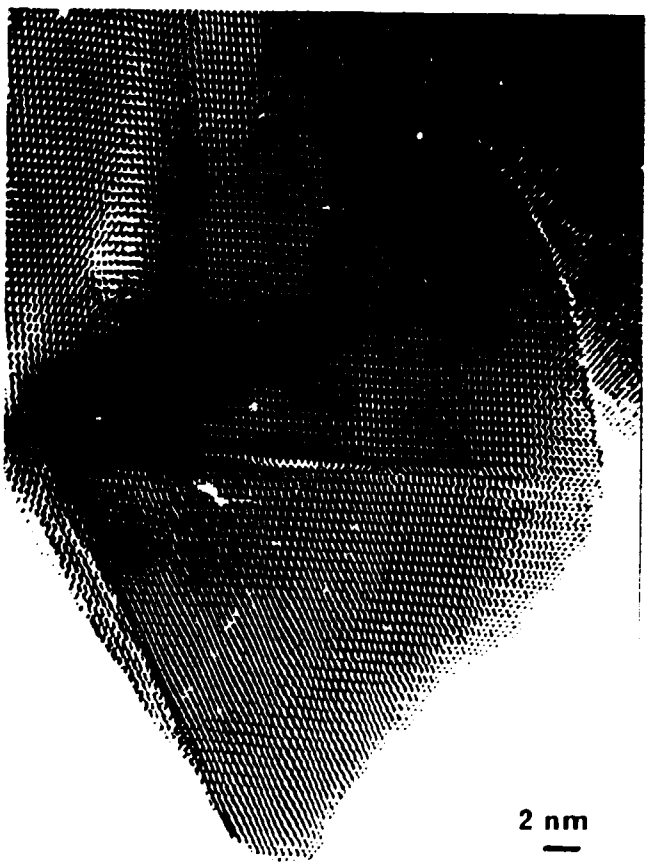

Fig 5

Fig 6

Fig 7a

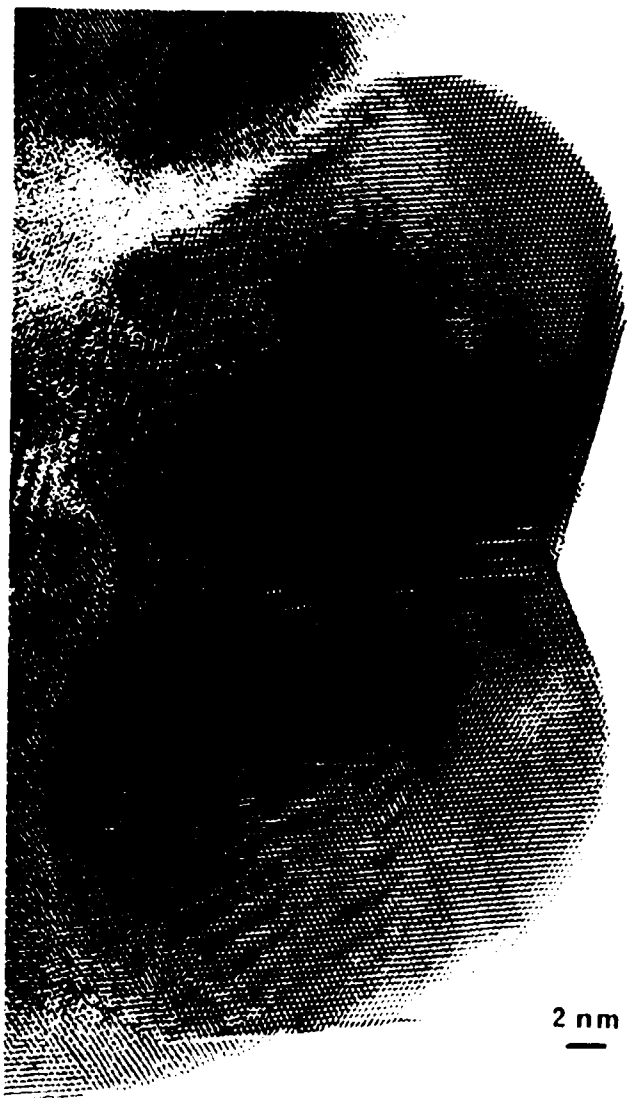

Fig 7b